32nd URSI GASS, Montreal, 19-26 August 2017

Investigation of Bandpass Filters in the Time Domain Signal Analysis of Reverberation Chamber

Qian Xu(1), Yi Huang(2), Yongjiu Zhao(1), Lei Xing(1), Zhihao Tian(2), and Tian Hong Loh(3)
(1) College of Electronic and Information Engineering, Nanjing University of Aeronautics and Astronautics, Nanjing 211106, China, emxu@foxmail.com
(2) Department of Electrical Engineering & Electronics, The University of Liverpool, Brownlow Hill, Liverpool, L69 3GJ, UK, yi.huang@liv.ac.uk
(3) Electromagnetic Technologies Group, Time, Quantum and Electromagnetics Division, National Physical Laboratory, Teddington, Middlesex, TW11 0LW, UK, tian.loh@npl.co.uk

Abstract

The time domain response of a reverberation chamber plays an important role in many applications. It is normally obtained from the inverse Fourier transform of the measured S-parameters in the frequency domain, and a bandpass filter (BPF) is normally used to select the frequency band of interest. However, the selection of the BPF has rarely been discussed and is a question in practice. In this paper, different types of BPFs are investigated, results from measurement data are given and compared. The interference from the input signal using different filters is quantified and it is found that the extraction of chamber decay constant is not sensitive to the type of employed filters. But for some applications the BPF selection is important.

1. Introduction

The time domain (TD) response of a reverberation chamber (RC) is extremely useful in many applications, such as the extraction of decay constant (τ_{RC}) [1], the antenna efficiency measurement [2], the absorption cross section measurement [3], the communication channel characterization [4], the scattering damping time extraction (τ_s) [5]-[7] and the stirrer efficiency qualification [6, 7].

In order to measure the TD response of the RC, frequency domain (FD) measurement is normally applied, because the FD measurement can offer a much larger dynamic range than the TD measurement and the TD response can be obtained from the inverse Fourier transform (IFT) of the measured FD response. In the RC measurement, BPF is used to filter the measured *S*-parameters, and then the IFT is applied to obtain the TD response of the filtered *S*-parameters. From the TD response, the decay constant τ_{RC} can be obtained by using the least square fit method [1] which is frequency dependent and the resolution depends on the passband of the used BPF. Elliptic filters were used in [2, 3, 6, 7] while rectangular filters were used in [8] without detailed discussion. This paper is focused on the BPFs used in the TD signal analysis of the RC; results are based on the practical measurement data. Conclusions are finally presented.

A schematic plot of a typical RC measurement is given in Fig. 1(a) and a typical measurement scenario is shown in Fig. 1(b). *S*-parameters can be measured by using a vector network analyzer (VNA), and then a BPF is used to select the frequency band of interest to process the collected *S*-parameters data. If one defines Port 1 as input port and Port 2 as output port, as depicted in Fig. 1(c), the BPF can be placed at the input port or the output port, although in measurement the *S*-parameters are normally measured first and BPF is applied later, they are actually equivalent ($F(j\omega) \times S21 = S21 \times F(j\omega) = \widetilde{S21}$). The BPF is placed at the input port in this paper to provide a better understanding. It is shown in Fig. 1(c) that, when the impulse signal ($\delta(t)$) is filtered by a BPF, a modulated impulse signal is obtained. The TD response from the IFT of $\widetilde{S21}$ is actually the response of a modulated impulse excitation.

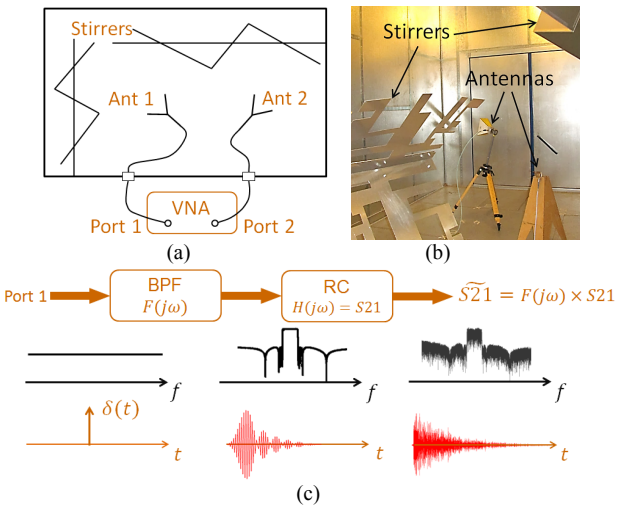

Figure 1. TD response measurement in an RC, (a) schematic plot of a typical measurement setup, (b) measurement setup at the University of Liverpool, (c) the use of a BPF to obtain the TD response of a modulated impulse input, $F(j\omega)$ is the transfer function of the BPF, $S21$ is the transfer function of the RC and $\widetilde{S21}$ is the total transfer function. FD spectrums are shown with frequency axis *f*, and the corresponding TD signals are illustrated with time axis *t*.

If we check Fig. 1(c) carefully, it can be found that, the input signal of the RC depends on the impulse response of the BPF. The extracted τ_{RC} is actually the average value in the passband of the BPF. It is expected to have a filter with a narrow passband in the FD and a short impulse response in the TD, so that the TD response of the RC will not be dominated by the input modulated impulse (impulse response of the BPF) and a good resolution of τ_{RC} and/or τ_s in the FD can be obtained. It is understandable that these two requirements cannot be ideally satisfied simultaneously as a short time signal in the TD means a wideband spectrum in the FD. An extreme case is that when the passband of the BPF is infinitely small (single frequency), the impulse response of the BPF is a continuous sine wave (infinitely long), the response of the RC will also be a sine wave which makes it impossible to observe the decay of the signal.

2. Bandpass Filters

In this section, we compare the performance of typical BPFs as it is impossible to enumerate all types of BPFs. *S*-parameters were measured in the RC at the University of Liverpool (Fig. 1(b)), 10001 points were recorded for each stirrer position in the frequency range of 2 GHz ~ 3.5 GHz, and 100 stirrer positions were used with 3.6 degrees/step. Typical measured *S*-parameters at one stirrer position are shown in Fig. 2. The detailed steps to extract the TD response and the decay constant are given below with different BPFs.

Rectangular filter: The rectangular BPF is a well-known filter which in the FD removes all frequency components outside the passband. Although the impulse response of the rectangular filter is non-causal, it does not affect the use of it, as we use it in the post processing of the measurement data rather than realize such a filter in practice. A rectangular filter with 100 MHz and 1.3 GHz passband are illustrated in Fig. 3(a), the corresponding normalized impulse responses can be obtained from the IFT of the FD response which are shown in Fig. 3(b). As expected, a wider passband BPF has a faster TD decay but the FD resolution is coarser. The power delay profile (PDP) can be obtained from $\langle |IFT(F(j\omega) \times S21)|^2 \rangle$, where $\langle \blacksquare \rangle$ means averaging for all stirrer positions, the normalized PDPs are shown in Fig. 3(c). The TD aliasing effect [1] can be well observed as the sampling interval in the FD is 150 kHz, which corresponds to 1/(150 kHz) = 6666.7 ns in the figures.

It can be observed in Fig. 3(b) that, when a 100 MHz BPF is used (the obtained PDP and τ_{RC} has a frequency resolutions of 100 MHz), the normalized input modulated impulse signal drops to -56 dB at 4000 ns (normalized to the peak value of 0 dB). Meanwhile, the PDP at 4000 ns is around -15 dB lower than the peak value. Ideally, the response should be purely from the RC and the input signal should decay to 0 ($-\infty$ dB) quickly. However, when the IFT is used to inverse the FD response, the decay of the input signal depends on the used BPF and there is always a finite tail for the input modulated impulse. This interference from the finite tail could lead errors when we analyze the TD response from the RC. An extreme case is that, when the input signal is a continuous sine wave (no decay or decay extremely slow), the output will also be a sine wave and no RC characteristics can be extracted.

By comparing Fig. 3(b) and Fig. 3(c), if we assume that the peak response (0 dB) of the PDP is from the peak magnitude of the input signal (TD impulse response of the BPF), it can be seen that the interference from the input signal is around 41 dB lower than the RC response at 4000 ns, the response from the RC dominates the TD response. The interference level from the input signal ($norm[IFT(F(j\omega)]$ (dB) $-$ $norm(PDP)$ (dB)) can be obtained from the difference between Fig. 3(b) and Fig. 3(c) and is shown in Fig. 4. As expected, the interference from the input signal is much smaller than the PDP in the whole time range, and the TD response is dominated by the RC but not the input signal.

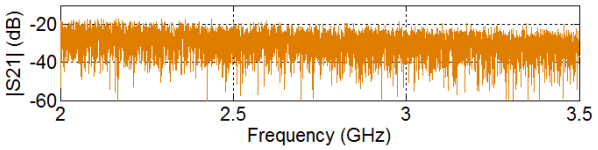

Figure 2. Typical measured S21 at one stirrer position.

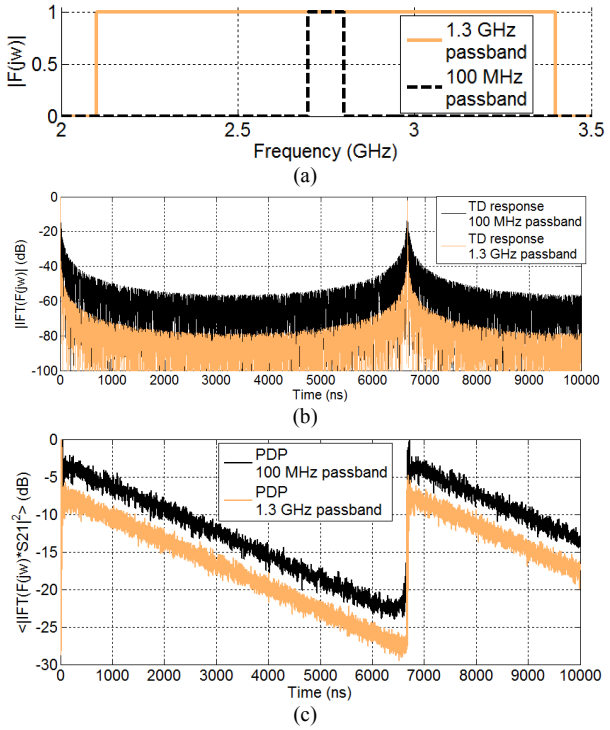

Figure 3. (a) Rectangular filter transfer functions $|F(j\omega)|$ in the FD, (b) the impulse response of the filter in the TD ($|IFT(F(j\omega))|$), only responses in positive time are plotted and normalized to peak value, (c) PDPs at the center frequency of 2.75 GHz, normalized to the peak value.

This rectangular filter has been used in the antenna radiation efficiency measurement in [8] and good results

were obtained. Fig. 4 is important, as it quantifies the interference from the input signal against the TD response of the RC. It should be noted that, although the interference shown in Fig. 4 is already very small in the τ_{RC} extraction, it could be significant in other applications, e.g. the extraction of the scattering damping time τ_s, because in the τ_s extraction, the decay speed of $|\langle IFT(F(j\omega) \times S21)\rangle|^2$ is much faster than $\langle |IFT(F(j\omega) \times S21)|^2 \rangle$ [6, 7]. As long as the interference level is quantified, a trustable region of the TD response of the RC can be identified.

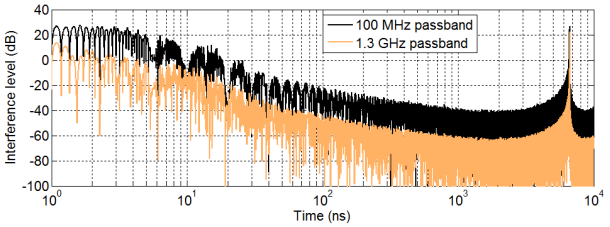

Figure 4. Interference level from the input modulated signal, horizontal axis is plotted in log scale to have a good resolution of early time.

Elliptic filter: The elliptic filter is famous for the sharpest transition between the passband and the stopband when compared with the same order Butterworth or Chebyshev filters. The same procedure is repeated for different orders of elliptic BPFs. As a high resolution in the FD is expected, we fix the passband as 100 MHz (the same as we used in the rectangular BPF), the transfer functions of different order elliptic BPFs are shown in Fig. 5(a), and the corresponding interference level from the input signal is given in Fig. 5(b). As can be seen, the interference level for low order elliptic filters decays faster than high order ones, and a large *Rs* means a low level tail (>100 ns). Compared to the rectangular filter (Fig. 4), for the same passband bandwidth, the elliptic filter can be better than rectangular filter in some applications.

Butterworth filter: The magnitude response of Butterworth filters is maximally flat in the passband and monotonic in the pass- and stopbands, while the sacrifice is the rolloff steepness between the pass- and stopbands. Typical transfer functions of Butterworth filters are shown in Fig. 6(a), interference levels are given in Fig. 6(b). As can be seen, Butterworth filters can also provide sharp early time decay and low level tail.

Chebyshev filter: Chebyshev BPFs (100 MHz passband, 0.3 dB ripples) have also been studied and the interference level (Fig. 7) is comparable with the Butterworth filter in Fig. 6(b), when the order becomes 8, the interference level roll off slower than the Butterworth filter.

Gaussian filter: Gaussian pulse has been widely used in the TD simulation in computational electromagnetics [9]; it can also be used in the inversion of TD signal in the RC (the RC is excited by a Gaussian pulse). A typical Gaussian BPF is shown in Fig. 8(a) with 100 MHz passband and the interference level is given in Fig. 8(b). As can be seen, the Gaussian pulse decays very fast in the TD compared with other filters, also the passband can be controlled easily in the FD, which proves the Gaussian filter can be a good candidate for the RC TD analysis.

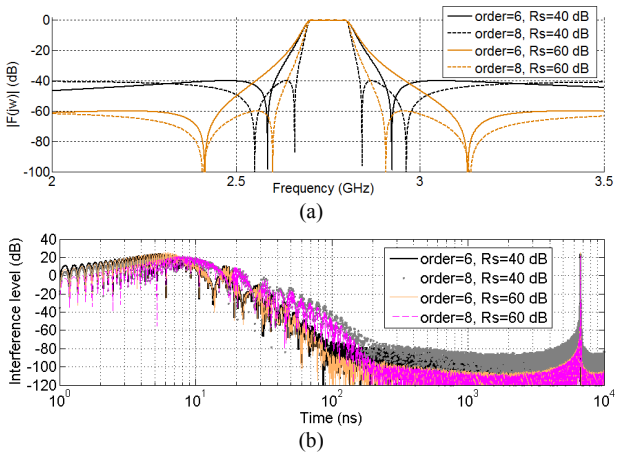

Figure 5. (a) Transfer functions of elliptic filters with 100 MHz passband, 0.3 dB ripples in the passband, *Rs* means the stopband is *Rs* dB down from the peak value in the passband (b) interference level from the input signal with different elliptic filters.

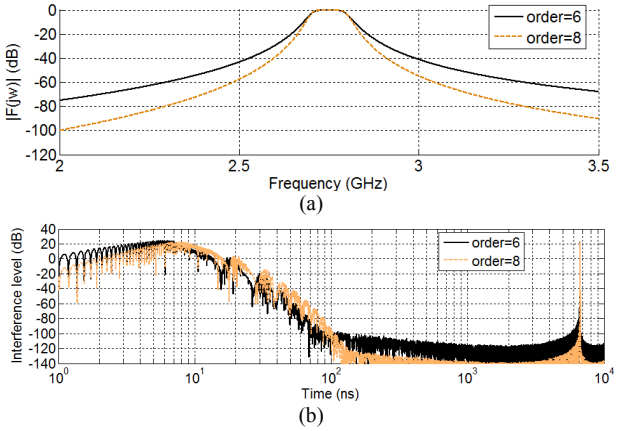

Figure 6. (a) Transfer functions of Butterworth filters with 100 MHz passband, (b) interference level from the input signal with different Butterworth filters.

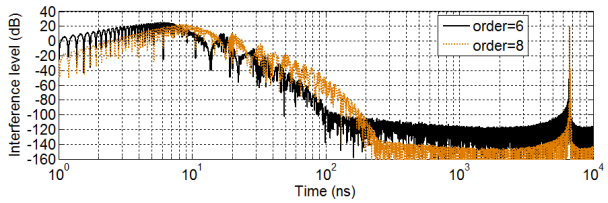

Figure 7. Interference level from the input signal with different Chebyshev filters.

By sweeping the center frequency of the BPF and applying the least square fit to the PDP [1] in the range of 500 ns ~ 5000 ns, the chamber decay constant can be extracted and shown in Fig. 9. As expected, all BPFs have very similar results and no significant difference is observed since all interference level is quite small. Even for the rectangular filter, it is smaller than -30 dB.

3. Conclusions

In the TD signal analysis of the RC, different BPFs have been studied in this paper to quantify their effects. It has been found that for an RC with long decay constant (τ_{RC}), the extracted τ_{RC} is not sensitive to the type of filters selected. A simple rectangular filter is good enough for most applications, however, in some applications, the effect of BPF could be significant such as investigating the early time behavior of the RC [10], scattering damping time measurement [5]-[7] and TSCS measurement [6, 7]. In these cases, Gaussian filter can be a good candidate and the interference level from the input signal needs to be checked to ensure the TD response is dominated by the RC but not the input signal.

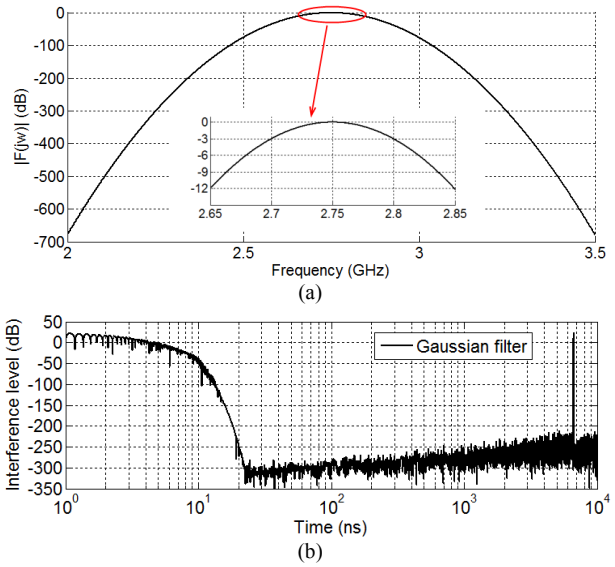

Figure 8. (a) Transfer function of a Gaussian filter with 100 MHz passband (-3dB), (b) interference level from the input signal with a Gaussian filter.

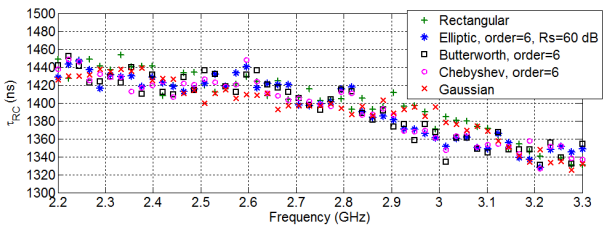

Figure 9. Extracted chamber decay constant by using different BPFs.

4. Acknowledgements

This work was supported in part by the National Natural Science Foundation of China (61601219) and Nature Science Foundation of Jiangsu Province (BK20160804). The work of T. H. Loh was supported by the 2016 – 2017 Quantum, Electromagnetics and Time Programme of the National Measurement Office, an Executive Agency of the U.K. Department for Business, Energy and Industrial Strategy, under Projects 119575.

5. References

1. Q. Xu, Y. Huang, L. Xing and Z. Tian, "Extract the decay constant of a reverberation chamber without satisfying Nyquist criterion," *IEEE Microwave and Wireless Components Letters*, **26**, 3, Mar. 2016, pp. 153-155, doi: 10.1109/LMWC.2016.2526027.

2. C. L. Holloway, H. A. Shah, R. J. Pirkl, W. F. Young, D. A. Hill and J. Ladbury, "Reverberation chamber techniques for determining the radiation and total efficiency of antennas," *IEEE Trans. Antennas Propag.*, **60**, 4, April 2012, pp. 1758-1770, doi: 10.1109/TAP.2012.2186263.

3. Z. Tian, Y. Huang, Y. Shen and Q. Xu, "Efficient and accurate measurement of absorption cross section of a lossy object in reverberation chamber using two one-antenna methods," *IEEE Trans. EMC*, **58**, 3, Jun. 2016, pp. 686-693, doi: 10.1109/TEMC.2016.2527363.

4. C. L. Holloway, D. A. Hill, J. M. Ladbury, P. F. Wilson, G. Koepke and J. Coder, "On the use of reverberation chambers to simulate a Rician radio environment for the testing of wireless devices," *IEEE Trans. Antennas Propag.*, **54**, 11, Nov. 2006, pp. 3167-3177, doi: 10.1109/TAP.2006.883987.

5. G. Lerosey and J. de Rosny, "Scattering cross section measurement in reverberation chamber," *IEEE Trans. EMC*, **52**, 2, May. 2007, pp.280-284, doi: 10.1109/TEMC.2007.893332.

6. Q. Xu, Y. Huang, L. Xing, Z. Tian, M. Stanley and S. Yuan, "B-scan in a reverberation chamber," *IEEE Trans. Antennas Propag.*, **64**, 5, May 2016, pp. 1740-1750, doi: 10.1109/TAP.2016.2535121.

7. Q. Xu, Y. Huang, L. Xing, Z. Tian, C. Song and M. Stanley, "The limit of the total scattering cross section of electrically large stirrers in a reverberation chamber," *IEEE Trans. EMC*, **58**, 2, Apr. 2016, pp.623-626, doi: 10.1109/TEMC.2016.2517038.

8. C. Li, T. Loh, Z. Tian, Q. Xu and Y. Huang, "A comparison of antenna efficiency measurements performed in two reverberation chambers using non-reference antenna methods," Antennas and Propagation Conference (LAPC), pp. 1-5, Loughborough, 2015, doi: 10.1109/LAPC.2015.7366141.

9. A. Taflove, *Computational Electrodynamics: The Finite-Difference Time-Domain Method*, 3rd ed, Artech House, 2005.

10. C. L. Holloway, H. A. Shah, R. J. Pirkl, K. A. Remley, D. A. Hill and J. Ladbury, "Early time behavior in reverberation chambers and its effect on the relationships between coherence bandwidth, chamber decay time, RMS delay spread, and the chamber buildup time," *IEEE Trans. EMC*, **54**, 4, Aug. 2012, pp. 714-725, doi: 10.1109/TEMC.2012.2188896.